Singular Features in Sea Surface Temperature Data

Q. Yang and B. Parvin
Computing Sciences
Lawrence Berkeley National Laboratory
Berkeley, CA 94720
http://vision.lbl.gov

A. Mariano
RSMAS
University of Miami
Miami, FL 33149

Abstract

We propose to detect singular features in order to generate an intelligent summary of high resolution spatio-temporal data that are obtained from satellite-based observations of the ocean. Toward this objective, we extend the Horn-Schunck model of flow field computation to incorporate incompressibility for tracking fluid motion. This is expressed as a zero-divergence constraint in the variational problem and an efficient multigrid implementation of it is introduced. Additionally, we show an effective localization of event features, such as vortices and saddle points, in the velocity field that can be used for subsequent abstraction, query and statistical analysis.

1 Introduction

Current environmental satellites provide oceanographic images with different types of telemetry data. The data is time-varying and often sparse. These data are calibrated and interpolated to generate dense geophysical fields, such as sea surface temperature (SST) data. Currently, the amount of raw data is a modest 3-4 Gigabytes/day, but it is expected to grow to 200Gbytes/day in the short term. Our aim is to create an intelligent summary of the time-varying data that also aids to observe short term oceanic evolution. Toward this end, we have focused to localize singular events, such as vortices and saddle points, from the spatio-temporal images. The ocean vortices are an important component of global circulation because they are an efficient transport and mixing mechanism for salt/freshwater, heat, plankton communities, nutrients, and momentum. On the other hand, saddle points are nonlinear points that are highly chaotic. Their presence has recently been noticed, which should aid in better understanding of ocean dynamics.

*This work is supported by the Director, Office of Science, Office of Advanced Scientific Computing Research, Mathematical, Information, and Computational Sciences Division of the U. S. Department of Energy under Contract No. DE-AC03-76SF00098 with the University of California. The publication number is LBNL-45734. Arthur J. Mariano was supported by the Office of Naval Research under grant N00014-95-1-0257.

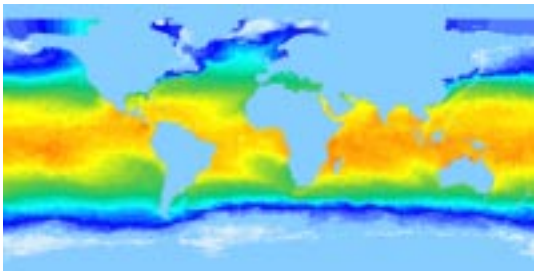

Figure 1. An example of SST image

Our focus is on extracting singular features from SST data. An example of SST data is shown in Figure 1. These singular points are computed from the underlaying feature velocities that are normal to iso-thermals. This work consists of two major parts: flow computation and feature detection. Our model of flow computation is novel in that it uses an incompressibility constraint to track fluid motion. This is a generalization of the classic optical flow model proposed by Horn and Schunck [6]. A multigrid strategy is then used for efficient implementation of the Euler-Lagrange equation. Singular points are then localized through the use of the Jordan curve index.

This paper is organized as follows. In Section 2, we review previous research in tracking fluid velocities and feature extraction. Sections 3 provide the details of our approach, including flow computation, feature detection, and experimental results on real data. Section 4 concludes the paper.

2 Previous Work

This section briefly reviews previous research in tracking of fluid motion and related work in feature extraction from vector field.

Measurement and analysis of feature velocities is often referred to computation of optical flow in the imaging literature. Review and enhancement of these techniques can be found in [3, 7]. However, tracking fluid motion poses additional constraints that has been addressed by only a few papers. In this context, we are not interested in tracking compressible fluid that focuses on clouds or images obtained from turbulent flows [9, 13]. These systems pose an affine model over the time varying imagery and ignore the inherent incompressibility constraint.

Cohen and Herlin [4] proposed a non-quadratic regularization technique for solving the optical flow constraint equation and applied it to oceanographic images. Their approach is applicable to irregularly spaced images with missing data. The regularization problem was solved by finite difference methods with finer tessellation near the motion boundary. Their method does not incorporate any constraints imposed by the fluid motion. Amini [1] extended the Horn-Schunck equation to include fluid X-ray images of contrast velocity in arteries. This was expressed in terms of zero divergence of flow field to *simplify* the solution. A major drawback of his approach is that the corresponding partial differential equations are of a higher order. Tistarelli [11] proposed an optical flow algorithm using multiple constraints in which a non-iterative least square estimation is used to compute the velocity vectors.

Raw oceanic data consists of satellite swath data and artifacts introduced by clouds. Modern oceanic processes perform cloud removal and time-space interpolation to produce dense data for daily, regional, and global fields. These data are then calibrated with in-situ measurements to produce a dense temperature map at each point on the oceanic grid. Dense oceanic data is the starting point for the proposed analysis that should satisfy the fluid incompressibility constraint. Additionally, because the data resides in the spherical coordinate system, special treatment is needed. Our formulation operates on dense data, does not require solution of higher order PDEs, and it has been implemented in a multigrid framework for better computational efficiency.

With respect to feature extraction from vector field, previous approaches rely on eigenvalue analysis from the local Jacobian [10, 12]. Our experience indicates that feature extraction is highly dependent on the smoothness of flow computation. If the flow field is regularized (as it is in our case) then events of interest can be easily localized. We will present an elegant approach for detection of vortices and saddle points that has proved to work effectively for our data sets.

3 Approach

This section outlines algorithms and their implementation for computing feature velocities from consecutive images of sea surface temperature data and to localize singular events (saddle points and vortices) from velocity fields.

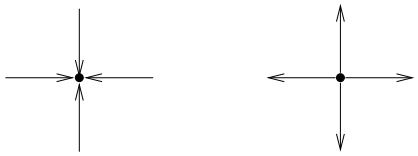

Figure 2. Critical points with non-zero divergence: (left) a sink; (right) a source.

3.1 Computation of feature velocities

Let $I(x, y, t)$ be the image at time t, with (u, v) as the velocity vector at each point. The flow field equation with brightness constancy assumption is given by:

$$\frac{dI(x,y,t)}{dt} = I_x u + I_y v + I_t = 0 \tag{1}$$

where the subscripts x, y, and t represent the partial derivatives. Horn and Schunck [6] constrained the problem by incorporating local smoothness in the flow. This is given by:

$$\begin{aligned}(u^*, v^*) &= \arg\min E := \int\int (I_x u + I_y v + I_t)^2 \\ &\quad +\alpha(|\nabla u|^2 + |\nabla v|^2) dx dy\end{aligned} \tag{2}$$

where α is the weighting factor of the smoothness term. Note that spherical coordinates should be used in this equation. We will discuss the problem of coordinate transformation later. The velocity vector due to (incompressible) fluid motion has to have zero divergence at each point:

$$u_x + v_y = -w_z \tag{3}$$

Since w is difficult to estimate, the above constraint is applied in a weak sense, e.g., $u_x + v_y = 0$. In this context, incompressibility is enforced along the temperature-gradient (normal to iso-thermals). A vector field with zero-divergence does not contain sinks and sources. A counter-example is shown in Fig. 2. This constraint is expressed as a penalty term in the energy functional:

$$\begin{aligned}(u^*_\beta, v^*_\beta) &= \arg\min E := \tfrac{1}{2}\int\int [(I_x u + I_y v + I_t)^2 \\ &+ \alpha(|\nabla u|^2 + |\nabla v|^2) + \beta(u_x + v_y)^2] dx dy\end{aligned} \tag{4}$$

If β is large enough, then (u^*_β, v^*_β) is a good approximation of the constrained optimization problem formulated as:

$$\begin{aligned}(u^*, v^*) &= \arg\min E := \int\int (I_x u + I_y v + I_t)^2 \\ &\quad +\alpha(|\nabla u|^2 + |\nabla v|^2) dx dy \\ &\quad s.t. \quad u_x + v_y = 0\end{aligned} \tag{5}$$

The Euler-Lagrange equations of (4) are

$$\begin{cases} -I_x(I_x u + I_y v + I_t) + (\alpha+\beta)u_{xx} + \alpha u_{yy} + \beta v_{xy} = 0 \\ -I_y(I_x u + I_y v + I_t) + \alpha v_{xx} + (\alpha+\beta)v_{yy} + \beta u_{xy} = 0 \end{cases} \tag{6}$$

To solve the above PDE-s, we will introduce an algorithm based on finite difference method below.

Recall that u's (and similarly v's) finite difference approximations are [8]:

$$\begin{aligned} u_{xx}|_{j,i} &= (u_{j+h,i} + u_{j-h,i} - 2u_{j,i})/h^2 \\ u_{yy}|_{j,i} &= (u_{j,i+h} + u_{j,i-h} - 2u_{j,i})/h^2 \\ u_{xy}|_{j,i} &= \tfrac{1}{4h^2}(u_{j+h,i+h} + u_{j-h,i-h} - u_{j+h,i-h} - u_{j-h,i+h}) \end{aligned} \tag{7}$$

Substituting them into Eq. (6), we have

$$\begin{cases} (I_x^2 + \frac{4\alpha+2\beta}{h^2})u_{j,i} + I_x I_y v_{j,i} = \Delta_1 \\ I_x I_y u_{j,i} + (I_y^2 + \frac{4\alpha+2\beta}{h^2})v_{j,i} = \Delta_2 \end{cases} \tag{8}$$

where

$$\begin{aligned} \Delta_1 &= -I_x I_t + \tfrac{\alpha+\beta}{h^2}(u_{j+h,i} + u_{j-h,i}) + \tfrac{\alpha}{h^2}(u_{j,i+h} + \\ & u_{j,i-h}) + \tfrac{\beta}{4h^2}(v_{j+h,i+h} + v_{j-h,i-h} - v_{j+h,i-h} - v_{j-h,i+h}) \\ \Delta_2 &= -I_y I_t + \tfrac{\alpha}{h^2}(v_{j+h,i} + v_{j-h,i}) + \tfrac{\alpha+\beta}{h^2}(v_{j,i+h} + \\ & v_{j,i-h}) + \tfrac{\frac{\beta}{h^2}}{4}(u_{j+h,i+h} + u_{j-h,i-h} - u_{j+h,i-h} - u_{j-h,i+h}) \end{aligned}$$

Representing $u_{j,i}$ and $v_{j,i}$ by Δ_1 and Δ_2, we have the following iterative method:

$$\begin{cases} u_{j,i}^{(n+1)} = \frac{1}{D}[(I_y^2 + \frac{4\alpha+2\beta}{h^2})\Delta_1^{(n)} - IxIy\Delta_2^{(n)}] \\ v_{j,i}^{(n+1)} = \frac{1}{D}[-IxIy\Delta_1^{(n)} + (I_x^2 + \frac{4\alpha+2\beta}{h^2})\Delta_2^{(n)}] \end{cases} \tag{9}$$

where $D = \frac{4\alpha+2\beta}{h^2}(Ix^2+I_y^2)+(\frac{4\alpha+2\beta}{h^2})^2$, $(u_{j,i}^{(n)}, v_{j,i}^{(n)})$ is the velocity field at the n-th step. If this process converges then (9) will become (8), which means that the optimal solution has been found. The convergency of the iteration defined by (9) is guaranteed, but due to space limitation, the proof is not given here. Note that if $\beta = 0$ then this formulation is identical to the original Horn-Schunck solution.

3.1.1 Multigrid approach

The solution to the above equations is achieved through multigrid technique to reduce the computational complexity. Let h be the window size where finite differences are computed. Then by setting $h = 2^K, 2^{K-1}, \cdots, 1$ successively, we can propagate from coarse to fine grid through simple linear interpolation and refinement. Linear interpolation is used because motion is locally smooth. It simply sets an initial condition for higher resolution computation to take place. This multigrid method can be described as follows:

- STEP 0. $h = 2^K$
- STEP 1. Repeat the following algorithm until it converges:

  for $(i = 0; i < M; i = i + h)$

  for $(j = 0; j < N; j = j + h)$ let

  $$\begin{cases} u_{j,i} = \frac{1}{D}[(I_y^2 + \frac{4\alpha+2\beta}{h^2})\Delta_1^{(n)} - IxIy\Delta_2^{(n)}] \\ v_{j,i} = \frac{1}{D}[-IxIy\Delta_1^{(n)} + (I_x^2 + \frac{4\alpha+2\beta}{h^2})\Delta_2^{(n)}] \end{cases}$$

  where $M \times N$ is the image size.
- STEP 2. Linear interpolation.

  for $(i = 0; i < M; i++)\{$

  $i_0 = [i/h] \cdot h, r_i = (i - i_0)/h;$

  for $(j = 0; j < N; j++)\{$

  $j_0 = [j/h] \cdot h, r_j = (j - j_0)/h;$

  $$\begin{aligned} u_{j,i} = \; & (1-r_i)(1-r_j)u_{j_0,i_0} + r_i(1-r_j)u_{j_0,i_0+h} + \\ & (1-r_i)r_j u_{j_0+h,i_0} + r_i r_j u_{j_0+h,i_0+h} \\ v_{j,i} = \; & (1-r_i)(1-r_j)v_{j_0,i_0} + r_i(1-r_j)v_{j_0,i_0+h} + \\ & (1-r_i)r_j v_{j_0+h,i_0} + r_i r_j v_{j_0+h,i_0+h} \end{aligned}$$

  $\}$ $\}$
- STEP 3. if $h = 1$, stop; else $h = h/2$, goto STEP 1.

Note that in STEP 1, all the pixels are updated asynchronously and not simultaneously. Why is the asynchronous iteration faster than the synchronous? An intuitive explanation is that the pixels that have been updated will be used to update their neighborhood. Even though this idea is rather simple, it can speed up the convergence greatly. In fact, it is a deterministic version of the classic Gibbs sampler [5].

3.1.2 Coordinate Transformation

Initially, we expressed relevant equations in the Cartesian, R^2, as opposed to the Spherical coordinate system, S^2, to simplify the PDEs. This was justified because data are high resolution (incremental longitude and latitude angles are small). However, by weighting the second derivatives with respect to their latitude, a closer results with ground truth data is obtained. The finite differences are expressed as:

$$\begin{aligned} u_{xx}|_{j,i} &= \tfrac{u_{j+h,i} + u_{j-h,i} - 2u_{j,i}}{h^2 \cos^2 i} \\ u_{yy}|_{j,i} &= \tfrac{u_{j,i+h} + u_{j,i-h} - 2u_{j,i}}{h^2} \\ u_{xy}|_{j,i} &= \tfrac{u_{j+h,i+h} + u_{j-h,i-h} - u_{j+h,i-h} - u_{j-h,i+h}}{4h^2 \cos i} \end{aligned}$$

where j and i are the longitude and latitude, respectively.

3.2 Evaluation of feature velocities

Both α and β of the regularization parameters are important for accurate measurement of feature velocities. There is a big difference between S^2 and R^2 in that their topological

structures are not homeomorphic. We have compared our measurements with ground truth data (obtained from surface drifters) and verified that our measurements are consistent. For example, from Nov. 5, 1986 to Nov 18, 1997, Aoki et al. [2] indicated a motion field of 3-5cm/sec to the west from 35° to 40° N in the region 30° to 40° N and 140° E to 170° W. Our measurements in the same area indicates a motion of 3.0 to 3.5 cm/sec.

3.3 Detection of vortices and saddle points

Singularities in the flow field can provide a compact abstraction in the velocity field. This issue has been addressed in literature [10], where an algorithm based on the analysis of local Jacobian was proposed. Their approach is complex due to the fact that the flow field is not regularized. Here, we propose an alternative method for robust estimation of event detection and subsequent tracking of singularities.

Let $F = (u, v)$ be a vector field and J be a Jordan curve with no critical point on it. The index of J is defined by

$$\text{Index}(J) = \frac{1}{2\pi} \oint_J \frac{udv - vdu}{u^2 + v^2}$$

Because it is not easy to localize the critical points, we compute the index over the entire field. At each point P, we choose a small circle J_P around P and compute Index(J_P). The flow field (u, v) can then be classified according to:

1. The index of a vortex is equal to $+1$ (the classification of singular points in a vector field is given in [10]), and
2. The index of a saddle point is equal to -1.

There is no node in the vector field because of the zero-divergence constraint, but singularities do occur. Recall that a point (x, y) is singular iff

$$\begin{cases} u(x, y) = 0 \\ v(x, y) = 0 \end{cases} \tag{10}$$

However, using the above equation to localize singularities leads to computational instability. A better approach is to exploit the inherent local minimum velocity volume to simplify the problem. Thus,

- Step 1: Find all local minimums of the velocity field:

  $S = \{$ All the local minimums of $\sqrt{u(x, y)^2 + v(x, y)^2}\}$

- Step 2: $\forall (x, y) \in S$:
  (1) Let $R = \frac{1}{2}\max\{r | S \bigcap J^r_{(x,y)} = \phi\}$ where $J^r_{(x,y)}$ is the circle centered at (x, y) with radius r.
  (2) Compute the index of $J^R_{(x,y)}$, that is,

$$\text{Index}(J^R_{(x,y)}) = \frac{1}{2\pi} \oint_{J^R_{(x,y)}} \frac{udv - vdu}{u^2 + v^2}$$

  (3) If Index($J^R_{(x,y)}$) $= 0$, then (x, y) is not singular; if Index($J^R_{(x,y)}$) $= 1$, then (x, y) is a vortex; if Index($J^R_{(x,y)}$) $= -1$, then (x, y) is a saddle point.

An Example of saddle points, observed in the Pacific, is shown in Figure 3. This result indicates that saddle points are not rare and they occur often in the oceanic flow. One important characteristic of vortex is its "size." Here, we propose a simple definition. If a point a (x, y) is a vortex, then its size $R^*(x, y)$ can be defined as:

$$R^*(x, y) = \max\{R | \text{Index}(J^R_{(x,y)}) = 1\}$$

that is to say, $R^*(x, y)$ is the largest R such that the index of $J^R_{(x,y)}$ keeps to be 1.

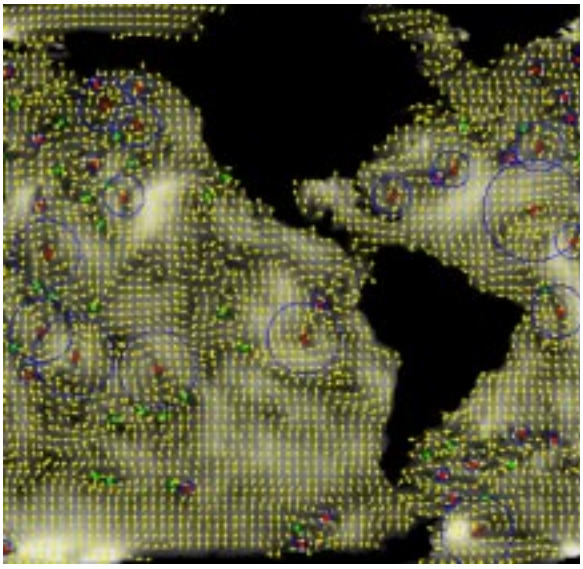

Figure 3. Feature velocity of SST (in yellow), magnitude of velocity (encoded with the underlying intensity), vortices and their size (in red block with blue circle for size), and saddle points (in green) on the 100th day of 1990.

3.4 Experimental Results

Fig. 4 shows the feature velocities (date: the 200th day of the year 1992) corresponding to a pair of SST data. Each vortex is marked by red blocks. A circle drawn around each vortex indicates its size. The direction of feature velocities are shown with yellow arrows. The magnitude of these velocity vectors are shown with the underlying intensity distribution.

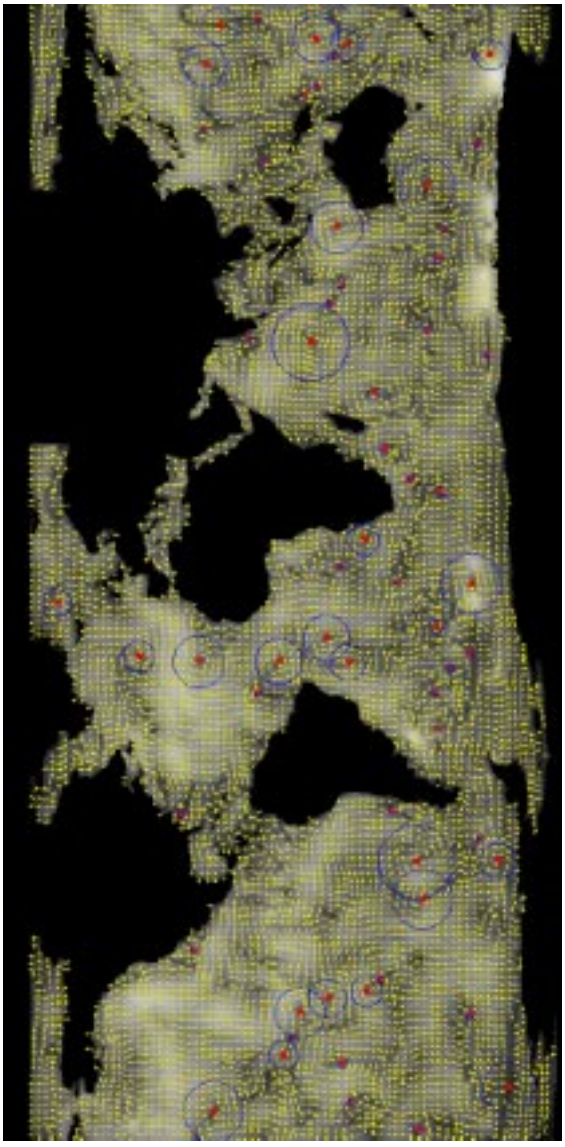

Figure 4. Feature velocities and computed vortices: Feature directions are shown with yellow arrows, and their corresponding magnitudes are shown with the underlying brightness map. Vortices are marked with a red block, and their size is encoded with a blue circle. This result is generated from a pair of consecutive images around day 200 from 1992.

4 Conclusions

In this paper, we formulated motion computation in oceanographic images as a constrained variational problem with incompressibility constraint, which is generalization of Horn-Schunck's original work. A simple approach for detection of singularities in the velocity field was proposed and implemented. The proposed singularities capture pertinent short term oceanic evolution so that long term climatic studies can be conducted in the feature space for better efficiency and information content.

References

[1] A.A. Amini. A scalar function formulation for optical flow: Application to x-ray imaging. In *IEEE Workshop on BioMedical Imaging*, pages A:117–124, 1994.

[2] S. Aoki, S. Imawaki, and K. Ichikawa. Baroclinic disturbances propagating westward in the kuroshio extension region as seen by a satellite altimeter and radiometers. *Geophysical Research-Oceans*, 100:839–855, 1995.

[3] J.L. Barron, D.J. Fleet, and S.S. Beauchemin. Performance of optical flow techniques. In *CVPR92*, pages 236–242, 1992.

[4] I. Cohen and I. Herlin. A motion computation and interpretation framework for oceanographic satellite images. In *SCV95*, pages 13–18, 1995.

[5] S. Geman and D. Geman. Stochastic relaxation, gibbs distribution and bayesian restoration of images. *PAMI*, 6:721–741, 1984.

[6] B. K. P. Horn and B. G. Schunck. Determining optical flow. *Artificial Intelligence*, 17:185–203, 1981.

[7] S.H. Lai and B.C. Vemuri. Robust and efficient algorithms for optical flow computation. In *SCV95*, pages 455–460, 1995.

[8] R.J. LeVeque. Finite difference methods for differential equations. *Math Note 585-6*, pages 225–270, 1998.

[9] M. Maurizot, P. Bouthemy, and B. Delyon. 2d fluid motion analysis from a single image. In *CVPR'98*, pages 184–189, Santa Barbara, California, 1998.

[10] A. R. Rao and R. C. Jain. Computerized flow field analysis: Oriented texture fields. *IEEE Transactions on Pattern Analysis and Machine Intelligence*, pages 693–709, 1992.

[11] M. Tistarelli. Computation of optical flow and it derivatives from local differential constraints. In *International Symposium on Computer Vision*, pages 19–24, Coral Gables, Florida, 1995.

[12] Y.L. Xiong and S.A. Shafer. Dense structure from a dense optical flow sequence. In *Intl. Symposium on Computer Vision*, pages 1–6, Coral Gables, Florida, 1995.

[13] L. Zhou, C. Kambhamettu, and D. Goldgof. Extracting nonrigid motion and 3d structure of hurricanes from satellite image sequences without correspondences. In *CVPR'99*, pages 281–285, Fort Collins, Colorado, 1999.